In-Situ Oxide Stabilization Development of Aluminum Foams in Powder Metallurgical Route

S. Asavavisithchai^{1,*} and Andrew R. Kennedy²

- Department of Metallurgical Engineering, Faculty of Engineering, Chulalongkorn University, Bangkok, Thailand
- ² Advanced Materials Research Group, School of Mechanical, Materials and Manufacturing Engineering, University of Nottingham, University Park, Nottingham, UK

Abstract. The development of stabilizing oxides during foaming process has been studied. The investigation of microstructure shows that the surface oxide films on the aluminum powder particles were ruptured after compaction. Pore nucleation results in a comprehensive shearing of oxides. After complete melting of powder particles at which a continuous liquid is dominant, the oxides move through the cell walls and Plateau borders by convection, due to pore growth, and connected to each other due to their tangled shape, forming strong local clusters or networks, leading to foam stability.

Keywords. Aluminum, metallic foam, oxides, powder metallurgy.

PACS® (2010). 81.05.Ni, 81.05.Bx, 81.05.Rm.

1 Introduction

Production of aluminum (Al) foam via powder metallurgy route requires a mixture of Al or Al-alloy powder and blowing agent, typically TiH₂, followed by compaction to high density and heat treated to a temperature above the melting point of the compact at which cellular structure is created [1]. This foaming process takes place in a few minutes before collapses to a steady state. It is thought that in-situ oxides, naturally obtained from Al powder surface, play a crucial role to stabilize foam structure in the same way as solid particles added to metal matrix composite (MMC) foams [2, 3]. Arnold et al. [4] pointed out that solid oxide networks are responsible for foam stability. A micro-gravity

Corresponding author: S. Asavavisithchai, Department of Metallurgical Engineering, Faculty of Engineering, Chulalongkorn University, Bangkok 10330, Thailand; E-mail: fmtsas@eng.chula.ac.th.

Received: September 17, 2010. Accepted: October 20, 2010.

experiment shows that the primary action of the solid stabilizing oxides is to prevent films from coalescing while their influence on viscosity must be less important [5,6]. Körner et al. [7] concluded that global oxide network is ruptured by bubble nucleation and bubble growth, leading to local oxides network particles which act as mechanical barriers against cell wall thinning. Numerical simulation based on a lattice Boltzmann model shows that a repulsive disjoining pressure responsible for foam stability is induced by particles confined in cell walls [8]. Ip et al. [9] suggests that the presence of solid particles in a liquid foam leads to flatter curvatures around the Plateau borders which reduces suction of liquid metal from the cell wall into the border. Particle additions to liquid-Al alloy can significantly decrease the surface tension of the liquid-metal dispersion [10].

Although the role of oxides on foam stabilization has been realized but it is still unclear about how oxides are distributed in foam structure and form a network. A good understanding of oxide network forming with foam structure development will lead to an improvement in foam quality. This study focuses on the development of oxide stabilization during foaming process.

2 Experimental Procedure

Air-atomized Al powder, supplied by Aluminum Powder Company Ltd (ALPOCO), with a purity of 99.7 % and D_{50} of 67 μ m was mixed with 0.6 wt. % of TiH₂ powder, obtained from Aldrich Chemical Ltd., with a purity of 99.6 % and D_{50} of 33 μ m, in a turbular mixer for 20 minutes and uni-axially cold compacted in a 22 mm diameter die to a pressure of 650 MPa. The mixture compact was placed in a cylindrical stainless steel mould and foamed in a pre-heated furnace at 1073 K. The foaming time was varied between 315 and 450 s, in intervals of 15 s, after which the foams were removed from the furnace and allowed to cool in air. The volume expansion of foamed samples was calculated following the same method used in a previous study [11].

The foamed samples were sectioned longitudinally using electro-discharge machining (EDM). A contrast between cell walls and pores is enhanced using a matt black paint spraying the sectioned surface of foamed samples for the study of foam macrostructure. The black paint covering the sectioned cell walls was then removed by light grinding on SiC papers leaving a good contrast.

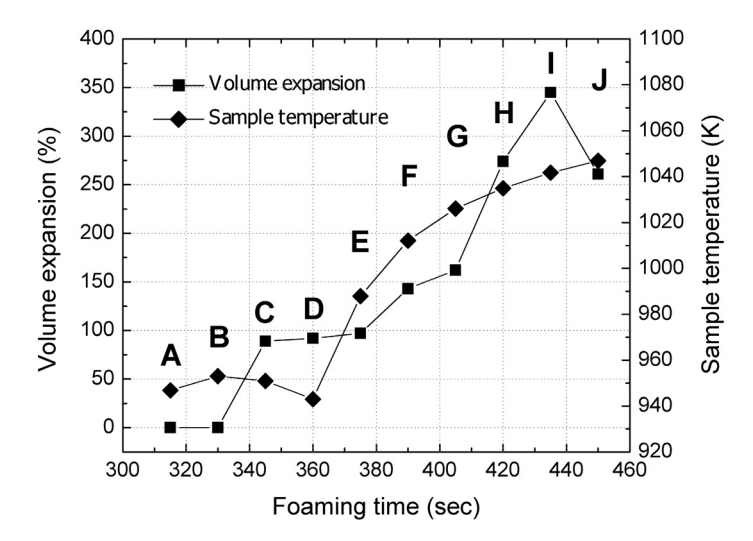


Figure 1. Foam expansion and sample temperature plots for interrupted foaming.

To study the foam microstructure, the sectioned samples were attached with an electrical contact at the back before mounting in cold-setting epoxy resin. The samples were ground and polished by using SiC papers with the grit of 400, 600, 800, 1200 and polished using diamond wheel up to 1 μm . The samples were subsequently anodized in a solution of 2 % HBF4 in water, for 45 s at 30 V, and viewing them in an optical microscope under cross-polarized light. Digital photos were recorded using a Nikon digital camera DXM1200F.

3 Results

Figure 1 shows plots of ex-situ foam expansion versus sample temperature. The onset of expansion is observed at a foaming time between 315 and 330 s. During this time, the temperature is close to the melting point of the precursor (933 K). The expansion increases significantly and continuously after a foaming time of 375 s, when the sample temperature reached about 988 K. The maximum expansion, of approximately 350 %, was achieved after foaming for 435 s and at a temperature of 1043 K. After the maximum expansion, the sample starts to collapse.

Figure 2.5 shows macrographs of foamed samples at various stages corresponding to time points on the foaming curve in Figure 1. The macrographs show pre-initiated pores (A), initiation of pores (B and C), pore growth (D, E, F, G and H) and pore collapse (I and J). No volume expansion and pores are seen before 315 s. During the onset of expansion, between 315 and 330 s, a few pores start to appear. The shape of the pores is crack-like, elongating perpendicular to the direction of compaction. The crack-like pores remain in the foamed samples until 375 s when the sample temperature remains between 933 and 953 K.

The pore morphology starts to change from crack-like to spherical shape and the size of pores increases with time. Before the maximum expansion of the foam, after foaming for between 420 and 435 s, a pore-free solid layer at the base of foam is observed. At the maximum expansion, after 435 s, several very large irregular pores appear and a clear density gradient between the top and bottom of the foam is observed. After the maximum expansion, a very thick pore-free solid layer develops at the base of foam. Most of the pores in the collapsed foam are large and irregular.

Figure 3 shows an optical micrograph of grain and oxide structure in an Al-TiH₂ precursor. No porosity is observed. The shapes of Al powder particles are deformed and elongated perpendicular to the compaction direction. The TiH₂ particles reside at the grain boundaries between the Al powder particles. No fracture of the hard and angular TiH₂ particles is observed. The black phase dispersed in the anodized optical micrograph is the oxide film present on the particle surfaces, which has been revealed and exaggerated in size by the anodizing process. The oxides are randomly distributed without significant clustering.

Figure 4 shows optical micrographs of the grain, oxide and pore structure development from stages A to J, corresponding to Figures 1–2. The development of grain and oxide stabilizing microstructure in the pre-gas release stage (stage A) is shown in Figure 4a. The microstructure remains largely similar to that in the as-compacted precursor. Although the temperature measured at this stage is higher than the theoretical melting point of the precursor, little or no melting of the precursor is observed.

The initiation of observable porosity starts at stage B, after 330 s and at 953 K, as shown in Figure 4b. These pores are often connected, forming what looks like cracks in the precursors, which tend to be elongated perpendic-

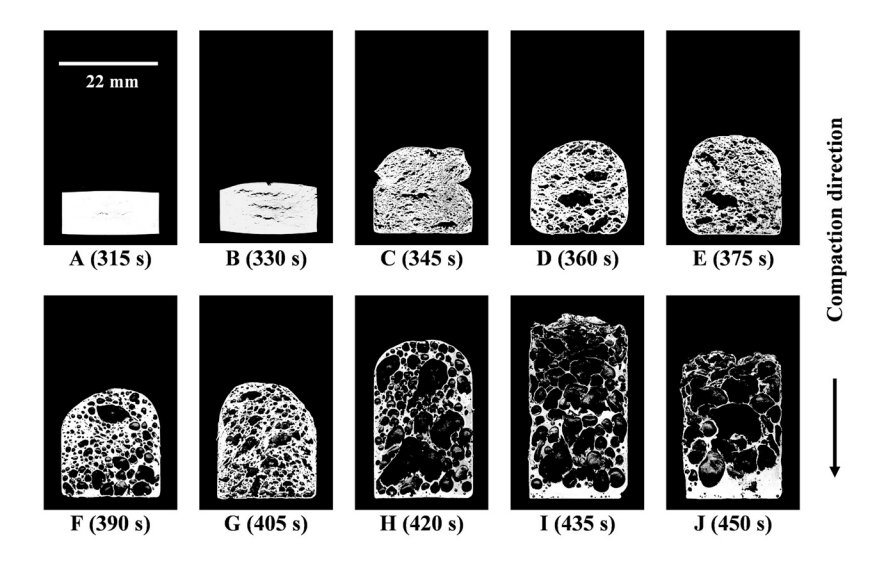


Figure 2. Macrographs showing the internal structure of foams heated for various times.

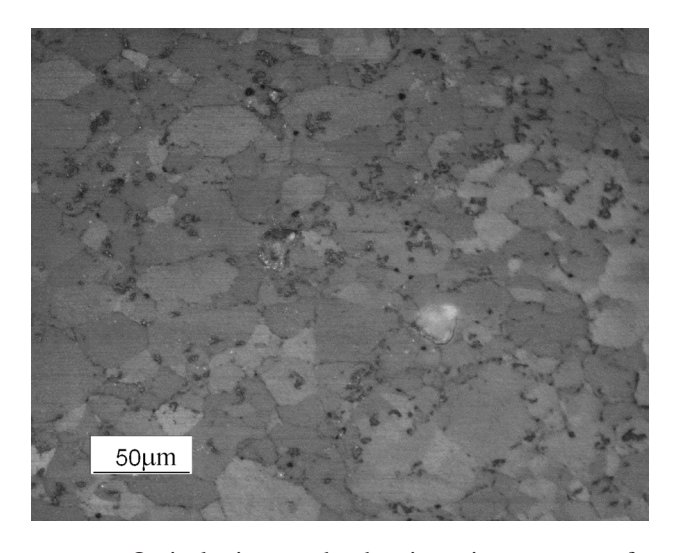


Figure 3. Optical micrographs showing microstructure of a precursor.

ular to the compaction direction. Small pores become connected via grain boundary channels and larger pores are created. Although a large number of pores are formed at this stage, each powder particle remains discrete and the oxide phases remain at the grain boundaries, indicating that melting has not yet taken place. At stage C, as shown in Figure 4c, after 345 s and at 951 K, the pores start to become larger and rounder. It is also at this point that melting was first observed. A higher magnification micrograph at this stage is depicted in Figure 5, where the powder structure containing many grains starts to disappear, powder particles start to merge and the oxides are no longer just observed at the powder boundaries.

A fully continuous liquid is not, however, formed by this stage.

Betweenstage D, after 360 s and at 943 K, and up to stage I, after 435 s and at 1042 K, as more hydrogen is evolved, foam expansion proceeds and the powder structure is lost, as shown in Figures 4d-i. During stage F, G, and H, the pores become more spherical and are enlarged by the increasing pressure of trapped gas. Complete melting of the powder is observed after stage G, 405 s and at 1026 K, as are the presence of a continuous liquid and a cast-type structure with a large grain size. Separation of dispersed oxides from the surfaces of the prior Al powder particles and clustering of these oxides in the bulk of the liquid are found to increase gradually, corresponding to increasing temperature and time. The dispersed oxides are observed to cluster locally close to the cell walls. An example of oxide clustering in the bulk liquid is presented in Figure 6. The oxide clustering tends to stay close to the cell wall and some oxides are observed to reside at the cell wall surface. At stage I, the cell walls achieve a minimum thickness of roughly 40-80 µm as the foam expands to a maximum of 350 %. A typical Plateau border at which three cell walls join together is illustrated in Figure 4i. Figure 7 shows an enlarged micrograph of a Plateau border and cell walls, and large grains and clustering of oxides are clearly observed. The oxide clusters are randomly distributed in both Plateau border and cell walls.

The collapse of the foam structure occurs after the maximum expansion is achieved, as shown at stage J in Figure 4j, after 450 s and at 1047 K. There are signs of heavy drainage, represented by a thick layer of liquid metal at the base of the sample and pore rupture and coalescence, evidenced by many large and irregular pores, as shown in Figure 2.

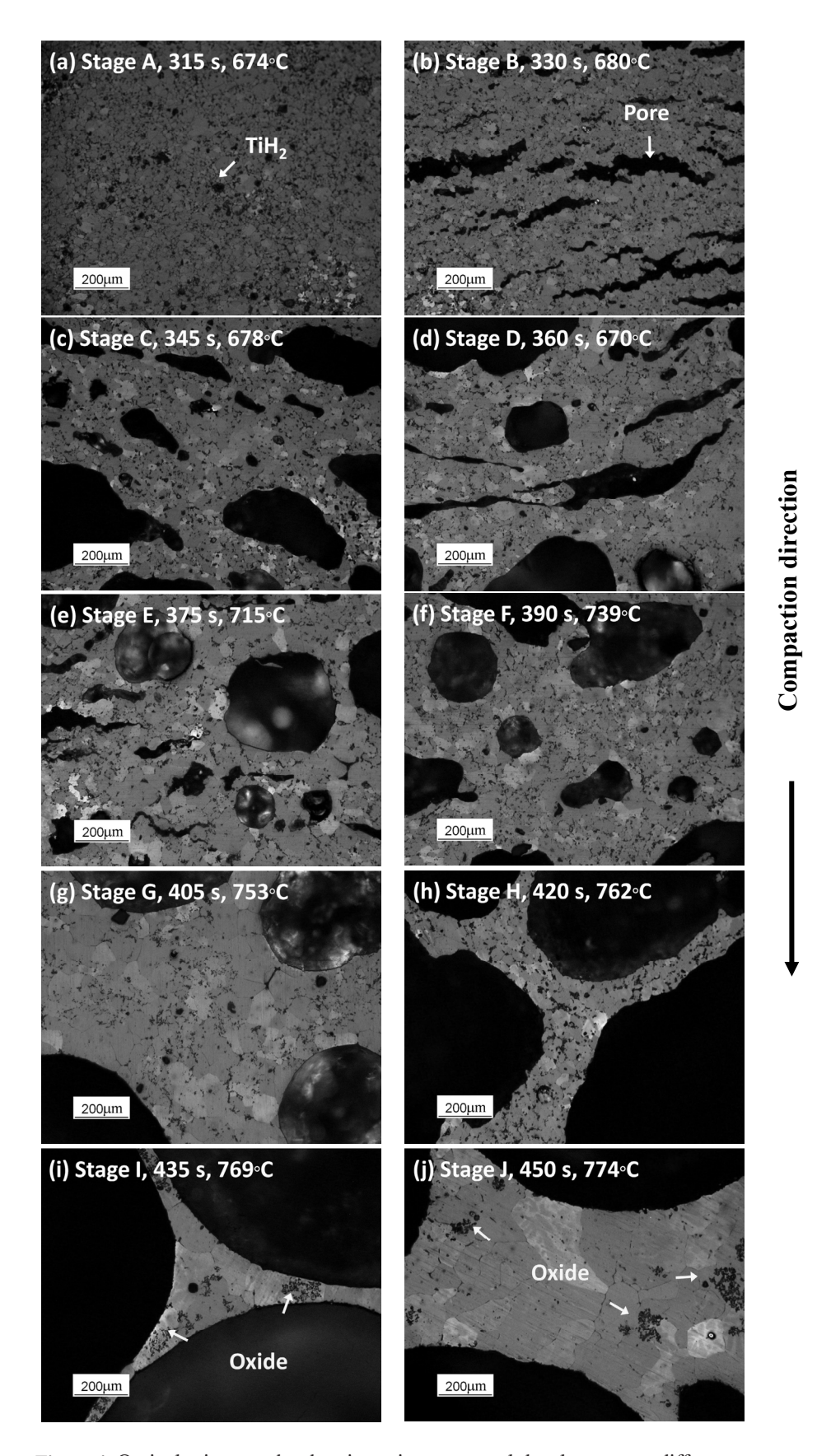


Figure 4. Optical micrographs showing microstructural development at different temperature and time.

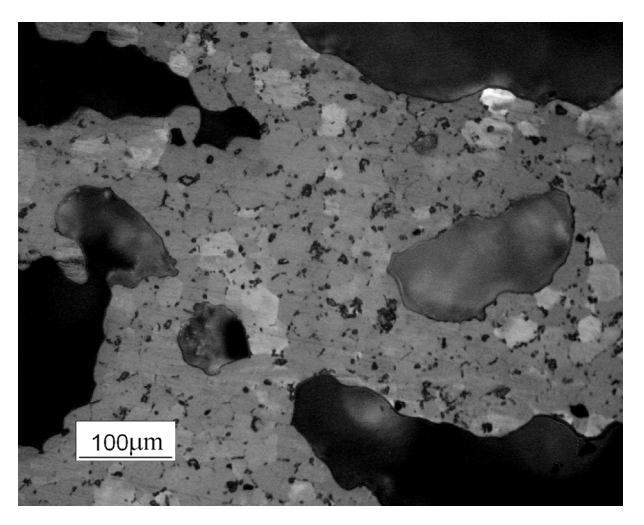


Figure 5. An optical micrograph showing the onset of melting of the powder particles.

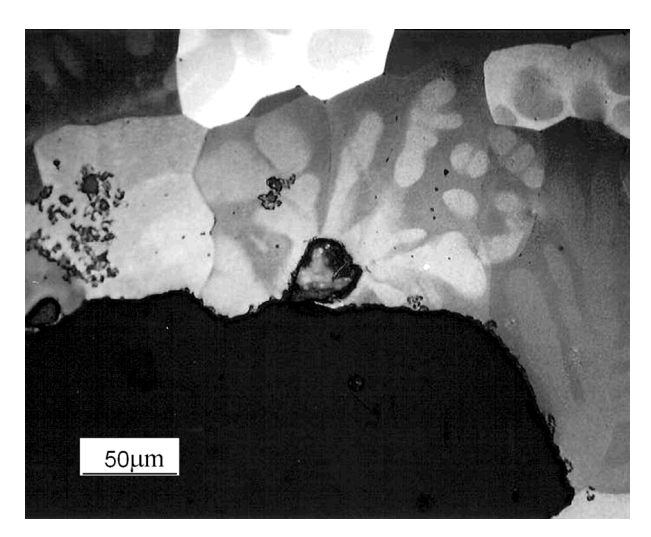


Figure 6. An optical micrograph showing oxide clusters close to cell wall surfaces.

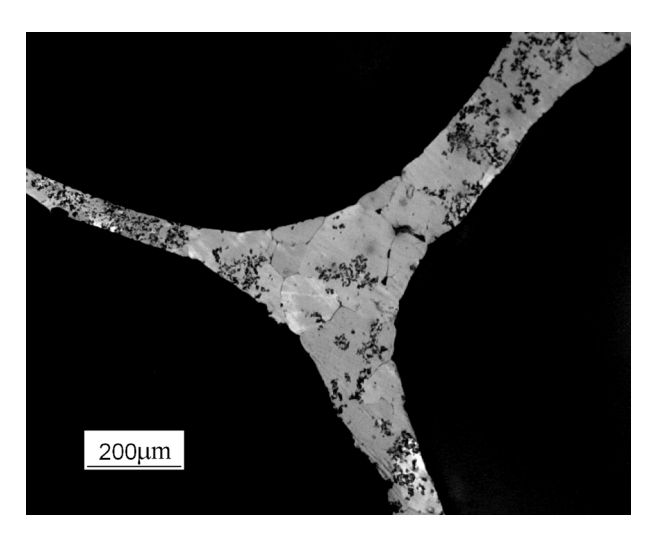


Figure 7. An optical micrograph showing the oxide clustering in cell walls and a Plateau border.

4 Discussion

4.1 Oxide Rupture

The surface oxide thickness for Al-alloy powders is reported to be in a range of 4-20 nm, depending upon atomizing gas, cooling rate and alloying elements [12]. The broken oxide films of Al powder particles, which are locally ruptured by shear stresses during uni-axial cold compaction to some degree [13], are predominantly dispersed along powder particle interfaces and on the particle surfaces in the precursors due to the inability of the compaction process to remove all the oxide from their original locations. The fresh underlying Al can penetrate through channels between ruptured oxides and meet with other fresh Al, resulting in cold welding. It is likely that small scale clustering and mechanical bonding of the ruptured oxides occurs, even though they are not clearly observed in the anodized precursors. Staniek [14] reported that ruptured surface oxides of Al-alloyed powder particle were separated from original particle surfaces and varied in shape, size and volume content. The oxides were mostly large coarse ductile films (>1 nm), which were folded or tangled and arranged into a three-dimensional structure. As foam expansion takes place, the oxide films are likely to be further ruptured due to extensive shearing. The ruptured oxides observed in this study, because of their large sizes, 1-5 µm, are thought to have been exaggerated by the anodizing process, and may show the areas within a tangled oxide film. The actual size of the oxides will be smaller.

4.2 Before Powder Melting

It is known that TiH₂ starts to decompose, releasing hydrogen gas, at approximately 673–723 K [15, 16] which is well below the melting temperature of Al (933 K). Although the sample temperature at stage A is slightly higher than the melting point of Al, there is insufficient time to melt the powder particles and the viscosity is still too high for the pores to expand. A similar microstructure of grain and oxide distribution to that of the as-compacted precursor indicates that the powder is still solid.

As the gas release continues, the pressure in pores increases and is relieved by penetration of gas along the grain boundaries. The pore formation, however, is still in the solid state. This is supported by the un-melted structure of powder grains that still widely exist. The anisotropic nature of pore nucleation and growth is clearly seen at this stage. The pore morphology that develops is not spherical but crack-like. This is results from an anisotropic microstructure of the pressed powders after uni-axial compaction which results in a higher strength of bonding perpendicular to the compaction direction [13], making gas flow easier in one direction. Increasing pressure from gas release of TiH₂ and increasing temperature during the foaming process facilitates further rupture of the oxide films.

4.3 Melting of Powder Particles

A sudden increase in porosity from stage B to C coincides with the onset of change in the powder structure to produce a liquid phase. The formation of numerous new pores is dominant in the early foaming stage, from stages C to D, the powder melts. This, however, results in only a small expansion, between 89 and 92 %, since the viscosity of the precursor is still high. The driving force for grain structural change in a powder system is to reduce the free energy of the system and reduce the surface area. At this stage, the particles are still discrete and grain boundaries between particles can still be seen. As temperature and time increase, contacts between particles grow and grain boundaries between the particles start to disappear. This is supported by microstructural observation of the grain structure, from stages C to D, which clearly indicates that grain growth occurs and grain boundaries become larger during this foaming interval. The powder structure is almost completely lost at stage D with evidence of a liquid phase forming in each particle. The sample temperature remains close to the Al melting point during this period, between stages C and D, because of the large latent heat required to melt the particles. Increasing the quantity of the liquid phase with time and temperature leads to a decrease in viscosity. A change in pore shape from crack-like to spherical is evident during this transition.

4.4 Formation of a Continuous Liquid

Significant foam expansion starts when the powder melts, after stage D. The presence of a large number of small pores is due to the reduction in the viscosity of the precursor which has allowed new pores to be nucleated. It is well known that the viscosity and surface tension of Al and Al alloys reduces with increasing temperatures [17, 18]. The formation of a continuous liquid and a decrease in the viscosity of the liquid allow spherical pores to be formed and expand. When the foam is in the fully liquid state, it is reasonable to assume that the mechanism for pore growth is similar to that for the traditional liquid foaming route. The flow of liquid throughout the foam via a network of cell walls and Plateau borders enables rapid expansion to occur.

The rapid and large-scale expansion, from stage E to I at which the maximum expansion of 345% is achieved, is likely to have been caused by pore growth from either individual or interconnected pores, from TiH₂ particles from which hydrogen gas was not yet depleted, rather than the nucleation of new pores [19]. It is after this point that the oxide phases are no longer able to pin the powder particles and transportation of oxides is possible. A continuous liquid phase forms in which the oxide networks are free to move, leading to oxide rearrangement. Disappearance of particle boundaries coupled with an extensive increase

in the grain size indicates that a continuous liquid phase is dominant.

It is reported that pore nucleation and growth mechanically break down the global oxide network to smaller oxide network particles [7]. The size and shape of oxide network particles depends on coagulation and fragmentation during the nucleation. However, the evidence obtained from the microstructure shows that oxide clusters forms when melting of powder particles is completed and continuous liquid is widespread. It is, therefore, thought that pore growth is mainly responsible to forming of oxide clusters whilst pore nucleation is responsible to shearing of oxides. Moreover, a large global oxide network is not observed in this study. It is likely that amount of oxide present in the foam was not sufficient to create a large network.

Figure 8 depicts a schematic of the formation of oxide clusters. The ruptured oxide films stay on the surface of the Al powder particles after compaction and remain dispersed at the same location before melting. Once a continuous liquid is formed, the oxides circulate in the liquid by convection, aided by the large expansion of foam, and mechanically lock together, forming a strong network of oxide clusters.

4.5 Foam Stabilization, Drainage and Collapse

Drainage of liquid through the foam structure is inevitable and is caused by gravity and capillary forces [20, 21]. The gravitational drainage results in a thick liquid layer at the base of foam, whilst the capillarity drainage leads to cell wall thinning and a rupture of the cell walls. Due to this fact, drainage occurs simultaneously with expansion. A rapid and increasing deterioration in the foam structure, from uniform pores to irregular pore shape and size, and a rapid accumulation of liquid metal at the base of the foam, observed near the maximum expansion throughout collapse, from stage H to J, suggests that the rate of drainage increases as a consequence of decreasing melt viscosity and increasing sample temperature. Further support for the consistent drainage with expansion is obtained from an observation of the micrographs, from stage C to J, during which the thickness of cell walls continuously reduces. A cell wall thickness of 40-80 µm at the maximum expansion, measured in the micrograph is in good agreement with other works for this type of foam [22].

The rate of drainage can be slowed down to some degree if there are some barriers present in cell walls and Plateau borders to block the passage of liquid flow and therefore stabilize the foam. In pure Al powder metallurgical foam systems, such barriers are the ruptured surface oxides [4]. During foam expansion, the oxides were observed to travel to the cell walls and Plateau borders via flow in the liquid. The oxides, therefore, become distributed throughout the continuous liquid. Additionally, the oxides tend to migrate

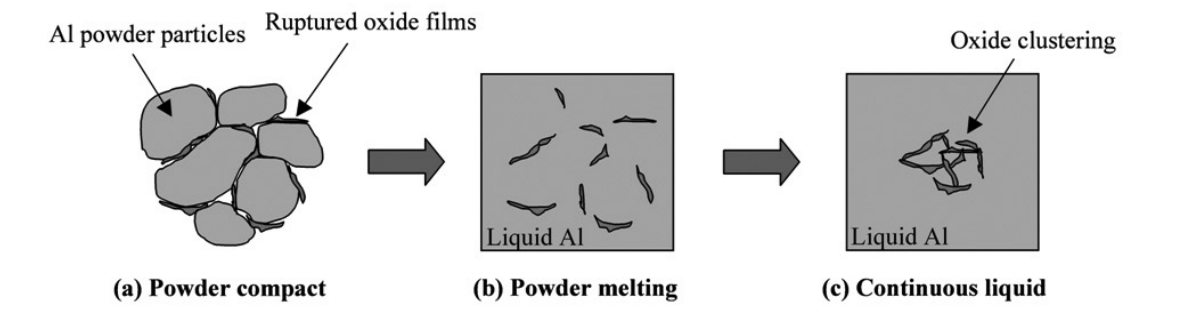


Figure 8. A schematic illustration showing the formation of oxide clustering.

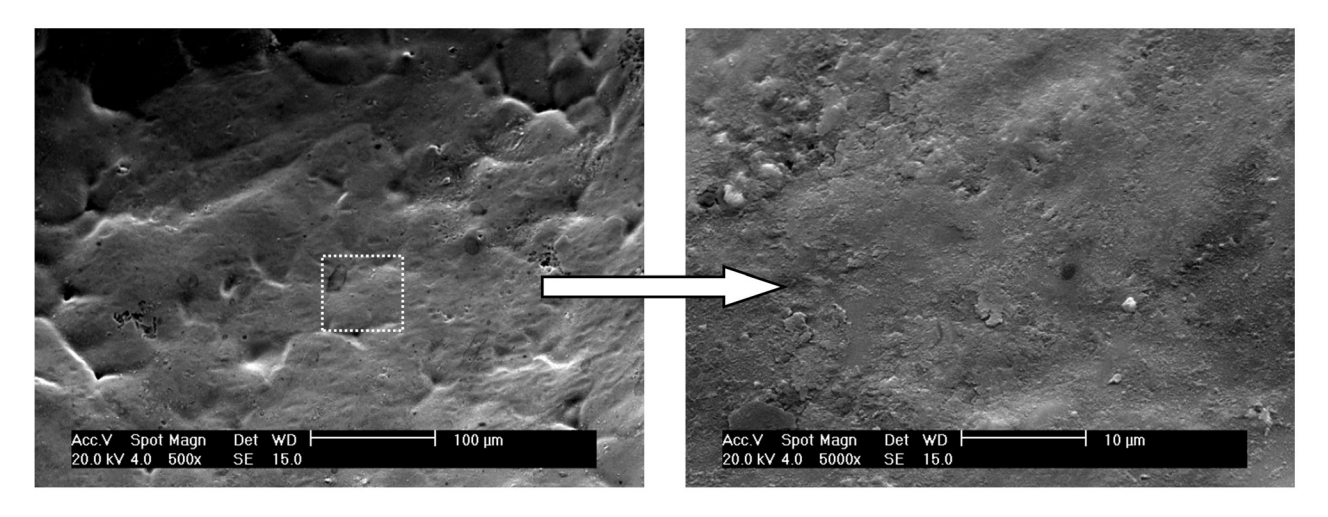


Figure 9. SEM micrographs showing cell wall surfaces of an Al foam.

to cell wall surfaces, due to their non-wetting nature (high contact angle). Contact angles between Al₂O₃ and Al have been reported to be in the range from 90° to 170° at 973 K [23-27], $\sim 160^{\circ}$ at 1073 K [28], $\sim 103^{\circ}$ at 1173 K [29] and \sim 63° at 1373 K [30]. A contact angle >90° indicates poor wetting. The oxides are, therefore, rejected from the liquid. It is expected that the oxide network will be completely wet by liquid Al due to a large internal surface of oxide network structure [7], but this is still in doubt. Figure 9 shows that the cell wall surfaces are indeed not smooth but comprise of small crumpled oxides when viewed in high magnification micrograph. The presence of the oxides in cell wall surfaces produce a decrease in the surface tension and an increase in the surface viscosity of the cell wall, and it is here that they can contribute to stabilizing the cell walls. It is reported that the oxide in foams plays a more crucial role in preventing cell wall rupture than in slowing drainage [5,6].

During this material redistribution process, the oxides inevitably become connected, resulting in local clustering. It is not well understood how connections between ruptured oxides are formed, but is likely that due to their tangled shapes, they are able to hook up to one another. If present at high enough a level, they can connect to form a threedimensional (3D) oxide network. It should be noted, however, that observation of a 3D oxide structure using optical microscopy and SEM in this study proved impossible. The oxide clusters observed in the present study are similar to interconnected oxide networks observed in other works [4,7], suggesting that the oxides can form a solid skeleton.

Although the presence of oxide helps stabilize the foam, consistent drainage after the maximum expansion occurs and is responsible for collapse. A decrease in foam expansion from 345 to 261 % indicates this. A large thick layer of liquid at the base of foam at stage J suggests that foam collapse resulted from gas loss to the environment by diffusion and cell wall rupture due to drainage.

A possible mechanism for foam expansion and stabilization by oxides is proposed as follows.

1. Shear from mechanical pressing ruptures oxide films on the powder surfaces during compaction. The fresh underlying Al can penetrate through channels between ruptured oxides and meet with other fresh Al, resulting in cold welding. The broken oxides remain at the powder particle boundaries and powder surfaces.

- 2. Increasing pressure from gas release of TiH_2 and increasing temperature during the foaming process facilitates further rupture of the oxide films. When the precursor becomes liquid and starts to expand, the oxides are able to move freely and connect with other oxides, and, if present in a high enough a level, form an extensive oxide network throughout the foam.
- 3. During progressive expansion, oxide tangling increases and more oxide networks are formed. The oxides in Plateau borders and cell walls result in an increase in the bulk viscosity of the liquid which retards the liquid flow, and therefore reduces the gravitational and capillary drainage. Oxides also migrate to the cell wall surfaces at which they reduce the surface tension and increase the surface viscosity of the cell walls, resulting in a decrease in capillary drainage.
- 4. The changes in the surface tension and surface viscosity of the cell walls, as well as structural strengthening of the cell walls by the presence of solid oxides, enabling large expansions to be sustained.
- 5. After the maximum expansion is reached, the foam starts to collapse as more pores coalesce, due to rupture of the cell walls.

5 Conclusions

Al foams produced via powder metallurgy route are stabilized by the surface oxide films on the Al powder particles. The oxide films are ruptured after compaction and largely remain along grain boundaries. During early stage of foaming, comprehensive shearing of oxides is driven by pore nucleation. When the structure becomes fully liquid, the oxides move through the cell walls and Plateau borders by convection, due to pore growth, and connected to each other due to their tangled shape, forming strong local clusters or networks. The presence of oxide clusters in the bulk of the liquid increases the melt viscosity and therefore reduces the rate of drainage, leading to foam stability. The migration of oxides to the cell wall surfaces leads to a decrease in the surface tension and an increase in the surface viscosity, which helps stabilize the cell walls.

References

- I. Duarte and J. Banhart, Acta Mater., 48(9) (2000), 2349– 2362.
- [2] A. R. Kennedy and S. Asavavisithchai, Adv. Eng. Mater., 6(6) (2004), 400–402.
- [3] A. R. Kennedy and S. Asavavisithchai, Scr. Mater., 50(1) (2004), 115–119.
- [4] M. Arnold, C. Körner and R. F. Singer, PM aluminium foams: stabilising mechanisms and optimization, in *Inter-*

- national Conference on Cellular Metals and Metal Foaming Technology, Berlin, Germany, 23–25. 6. 2003, MIT Verlag, pp. 71–76.
- [5] T. Wübben, H. Stanzick, J. Banhart and S. Odenbach, J. Phys. Condens. Matter., 15 (2003), 427–433.
- [6] T. Wübben, J. Banhart, and S. Odenbach, *Microgravity Sci. Tech.*, 13(3) (2002), 36–42.
- [7] C. Körner, M. Arnold and R. F. Singer, *Mater. Sci. Eng.*, A, 396(1–2) (2005), 28–40.
- [8] C. Körner, Mater. Sci. Eng., A, 495(1-2) (2008), 227-235.
- [9] S. W. Ip, Y. Wang and J. M. Toguri, Can. Metall. Q., 38(1) (1999), 81–92.
- [10] N. Babcsán, D. Leitlmeier and H. P. Degischer, *Material-wiss. Werkstofftech.*, 34(1) (2003), 22–29.
- [11] A. R. Kennedy, *Powder Metall.*, **45(1)** (2002), 75–79.
- [12] J. W. Bohlen, S. G. Roberts, and G. R. Chanani, *Investigation of improved methods for consolidating rapidly solidified aluminum alloy powder*, Northrop Corporation, Hawthorne, California (1982).
- [13] Y. W. Kim, W. M. Griffith and F. H. Froes, *JOM*, 37(8) (1985), 27–33.
- [14] G. Staniek, Observation of oxide skin in powder metallurgy aluminum alloys, Technical Report, Air Force Wright Aeronautical Laboratories, Ohio (1984).
- [15] F. Baumgärtner, I. Duarte, J. Banhart, Adv. Eng. Mater., 2(4) (2000), 168–174.
- [16] A. R. Kennedy, Scr. Mater., 47(11) (2002), 763–767.
- [17] A. T. Dinsdale and P. N. Quested, J Mater. Sci., 39 (2004), 7221–7228.
- [18] B. J. Keene, Inter. Mater. Reviews, 38(4) (1993), 157–192.
- [19] L. Helfen, T. Baumbach, H. Stanzick, J. Banhart, A. El-moutaouakkil and P. Cloetens, Adv. Eng. Mater., 4(10) (2002), 808–813.
- [20] V. Gergely and T. W. Clyne, Acta Mater., 52(10) (2004), 3047–3058.
- [21] V. Gergely, R. L. Jones and T. W. Clyne, *Trans. JWRI*, 30 (2001), 371–376.
- [22] Kriszt, B., P. Cekan, and K. Faure, Foamability of the Al-Si system, in *International Conference on Cellular Metals and Metal Foaming Technology*, Berlin, Germany, 23–25. 6. 2003, MIT Verlag, pp. 77–82.
- [23] S. M. Wolf, A. P. Levitt and J. Brown, *Chem. Eng. Progress*, 62(3) (1966), 74–78.
- [24] J. J. Brennan and J. A. Pask, J Am. Ceram. Soc., 51(10) (1968), 569–573.
- [25] H. John and H. Hausner, J Mater. Sci. Lett., 5(5) (1986), 549–551.
- [26] V. Laurent, D. Chatain, C. Chatillon and N. Eustathopoulos, *Acta Metall.*, 36(7) (1988), 1797–1803.
- [27] D. J. Wang and S. T. Wu, Acta Metall. Mater., 42(12) (1994), 4029–4034.
- [28] Y. Liu, Z. He, G. Dong and Q. Li, J Mater. Sci. Lett., 11 (1992), 896–898.
- [29] S. W. Ip, M. Kucharski and J. M. Toguri, J Mater. Sci. Lett., 12(21) (1993), 1699–1702.
- [30] G. Kaptay, E. Bader and L. Bolyan, Interfacial forces and energies relevant to production of metal matrix composites, in *Proceedings of the Third International Conference on Solidification and Gravity*, Miskolc, Hungary, 25–28 April 1999, Trans Tech Publications, Zurich-Uetikon, Switzerland (2000), pp. 151–156.